Published in final edited form as:

*Bioconjug Chem*. 2019 January 16; 30(1): 169–183. doi:10.1021/acs.bioconjchem.8b00820.

# Activatable Near-Infrared Fluorescence Imaging Using PEGylated Bacteriochlorin-Based Chlorin and BODIPY-Dyads as Probes for Detecting Cancer

**Fusa Ogata**[1], **Tadanobu Nagaya**[1], **Yasuhiro Maruoka**[1], **Joshua Akhigbe**[2], **Adam Meares**[2], **Melisa Lucero**[2], **Andrius Satraitis**[2], **Daiki Fujimura**[1], **Ryuhei Okada**[1], **Fuyuki Inagaki**[1], **Peter L. Choyke**[1], **Marcin Ptaszek**[2], **Hisataka Kobayashi**[1,*]

[1]Molecular Imaging Program, Center for Cancer Research, National Cancer Institute, National Institutes of Health, Bethesda, Maryland, 20892, United States of America

[2]Department of Chemistry and Biochemistry, University of Maryland, Baltimore County, Baltimore, Maryland 21250 United States of America

## Abstract

Near infrared (NIR) fluorescent probes are attractive tools for biomedical *in vivo* imaging due to the relatively deeper tissue penetration and lower background autofluorescence. Activatable probes are turned on only after binding to their target, further improving target to background ratios. However, the number of available activatable NIR probes is limited. In this study, we introduce two types of activatable NIR fluorophores derived from bacteriochlorin; chlorin-bacteriochlorin energy-transfer dyads and boron-dipyrromethene (BODIPY)-bacteriochlorin energy-transfer dyads. These fluorophores are characterized by multiple narrow excitation bands with relatively strong emission in the NIR. Targeted bacteriochlorin-based antibody or peptide probes have been previously limited by aggregation after conjugation. Polyethylene glycol (PEG) chains were added to improve the hydrophilicity without altering pharmacokinetics of the targeting moieties. These PEGylated bacteriochlorin-based activatable fluorophores have potential as targeted activatable, multi-color NIR fluorescent probes for in vivo applications.

### Keywords

Molecular imaging; Bacteriochlorin; Monoclonal antibody; Cancer

## INTRODUCTION

Fluorescence imaging is used in a variety of medical applications including fluorescence-guided surgery and endoscopy because it provides improved visualization of lesions in real time while using relatively affordable, portable equipment. Moreover, this is achieved without exposure to ionizing radiation.[1, 2] To achieve these goals the tumor to background

*Corresponding Author: Hisataka Kobayashi, M.D., Ph.D., kobayash@mail.nih.gov.

CONFLICT OF INTEREST

The authors declare no competing financial interest.

ratio (TBR) must be optimized by either maximizing signal from the target or minimizing signal from the background.[3, 4] There are several strategies for optimizing TBR of fluorescent probes.

Conventional fluorophores are “always-on” because they fluoresce regardless of the environment they are in or if they are bound or unbound. The TBR of such probes relies on the probe rapidly accumulating in the tumor while the background tissue clears the probe rapidly.[5–7] However, in reality, the TBR of such probes is inherently limited by clearance. In order to overcome this limitation, “activatable” fluorescence probes have been developed. Activatable fluorescence probes yield maximal signal only after binding to their targets while unbound probes yield no signal. Activating mechanisms include H- or J-dimer formation, Förster resonance energy transfer (FRET) or photo-induced energy transfer (PeT).[7] Activatable probes have recently been investigated in preclinical animal studies and several clinical trials.[8–10] An example of such a probe is one that consists of a peptide backbone which holds NIR emitting cyanine fluorophores in the quenched state. Upon exposure to a tumor environment containing employs a cathepsin-B, cathepsin-L[11, 12] or matrix metalloproteinases-2 (MMP-2) the probe dequenches allowing tumor visualization against a dark background[13, 14]

The use of NIR fluorescence is advantageous for *in vivo* imaging because NIR light penetrates further into tissue than other optical wavelengths which are rapidly absorbed by tissue. At the same time there are relatively fewer NIR autofluorophores in tissue, resulting in reduced autofluorescence.[2] NIR fluorophores, such as cyanine dyes (Cy5, Cy7), indocyanine green dyes (ICG), Alexa Fluor dyes (660–790 nm), SRfluor dyes, porphyrin dyes, phthalocyanine dyes, and hydro-porphyrin dyes including chlorin and bacteriochlorin, have been developed for biomedical applications and many are commercially available.[15]

Bacteriochlorin dyes are particularly promising fluorophores.[16, 17, 18] For instance, bacteriochlorins conjugated to galactosyl-human serum albumin (hGSA) is normally quenched. After binding to H-type lectin on the cell surface of ovarian cancer metastases, conjugate dequenches depicting the sites of cancer.[19, 20] However, this compound will only work well in peritoneal metastases. To improve the generalizeability of bacteriochlorin dyes, attempts have been made to conjugate them to antibodies but such conjugates exhibited marked hydrophobicity and aggregation.

Chlorin-bacteriochlorin energy-transfer dyads[21, 22] and BODIPY–bacteriochlorin energy-transfer dyads[23, 24] are newly developed NIR fluorescence probes based on the bacteriochlorin platform. In chlorin-bacteriochlorin energy-transfer dyads, chlorin is an energy donor and bacteriochlorin is an energy acceptor (NMP6 and NMP7, Figure 1A). Excitation of the chlorin results in relatively strong emission of light from the bacteriochlorin via energy transfer.[22] Additionally, chlorin and bacteriochlorin are hydroporphyrins and the emission band is relatively narrow while the peak can be precisely tuned by a simple substitution on the macrocycle periphery.[25] BODIPY–bacteriochlorin energy-transfer dyads, in which BODIPY is employed as an energy donor (NMP11 and NMP12, Figure 1B) and bacteriochlorin as the acceptor has additional properties. BODIPY possesses higher hydrophilicity and a superior extinction coefficient in the green light

window than does chlorin.[24] However, since these dyes contain bulky ring structures that makes them hydrophobic, oligo polyethylene glycol (PEG) chains are needed to improve their solubility and alter their pharmacokinetics.

This study aimed to evaluate the relative performance of these activatable NIR bacteriochlorin-based fluorophores after PEGylation to improve their utility in *in vivo* cancer imaging.

## RESULTS

### Molecular design and synthesis of fluorophores

The molecular design of amphiphilic chlorin-bacteriochlorin energy transfer arrays **NMP6** and **NMP7** (Figure 1A), was based on previously published results for hydrophobic chlorin-bacteriochlorin arrays,[21] and amphiphilic BODIPY-hydroporphyrin arrays,[23] as well as recent progress in the synthesis of water-soluble chlorin derivatives.[26] As energy donors hydrophilic chlorin was used which was altered by the addition of three oligoethylene glycol (a kind of PEG) substituents, installed at the 2,4,6-positions of the aryl group located at the 10-chlorin position. In that way, PEG substituents are positioned above and below the chlorin plane, preventing aggregation and increasing water solubility in the case of chlorin monomer.[26] Two different bacteriochlorins were employed as energy acceptors, one with two aryl substituents (absorption at 736 nm and emission at 744 nm)[23] and a second with two diarylacetylene substituents (absorption at 761 nm and emission at 766 nm). In both arrays the linker is connected to the 3-chlorin position and 13-bacteriochlorin position.

Synthesis of chlorin monomers follows the reported procedure for analogous chlorins, described previously.[26] Thus, condensation of dipyrromethane **DPM-1**[26] with 8-bromotetrahydrodipyrrin **THD-1**[27] provides target chlorin **ZnC1** in 16% yield and **ZnC2**, lacking one propargyl group (Scheme 1). The latter can be nearly quantitatively converted into **ZnC1** in reaction with propargyl bromide (Scheme 1). PEG substituents were installed on **ZnC1** using a microwave-assisted click reaction[23, 26] using triethylene glycol azide **3PEG-$N_3$**[28] or tetraethylene glycol azide, **4PEG-$N_3$**,[29] and subsequent *in situ* de-metalation of the resulting zinc complexes to obtain **C3** and **C4** in 68% and 83% yield, respectively (Scheme 2). The syntheses of dyads was initially attempted using a method analogous to that employed previously for hydrophobic dyads, i.e. EDC-mediated amide formation between an acid-functionalized chlorin, and amine-functionalized bacteriochlorin. Thus, Suzuki reaction of **C3** and **C4** with 4-(methoxycarbonyl)phenylboronic acid pinacol ester provides chlorin esters **C5** and **C6** in 82% and 76% yield, respectively (Scheme 2). Hydrolysis of the ester group in **C5** and subsequent reactions of resulting acids with **BC1**[23] in the presence of EDCI provides **NMP6-OMe** in 33% yield, accompanied by several by-products (Scheme 3). An analogous reaction using acid obtained from the hydrolysis ester function in **C6** and **BC2** provides only traces of dyad **NMP7-OMe** (Scheme 3). Attempts to improve the yield of amide formation using different coupling agents (i.e. HATU, or CDMT/NMM)[27] were unsuccessful. Therefore, we pursued an alternative route, whereby we utilized a previously described bacteriochlorin with boronic ester functionality **BC4**,[23] and conjugated both chlorins and bacteriochlorins through the Suzuki reaction. Thus, reaction of **C4** with **BC3**

under standard Suzuki conditions[30] **NMP7-OMe** was found in 12% yield (Scheme 4). Ester functionality in dyads, **NMP6-OMe** and **NMP7-OMe,** which were hydrolyzed and NHS ester were installed in reaction with *N*-hydrosuccinimide, in the presence of EDCI, to obtain **NMP6** and **NMP7** in nearly quantitative yields.

Syntheses of BODIPY-bacteriochlorin dyads methyl esters of NMP11 and NMP12 (Figure 1B), and their full spectroscopic characterization, were reported previously.[23] The NHS-esters were prepared by basic hydrolysis of corresponding methyl esters, and reaction of the resulting acids with *N*-hydroxysuccinimide in the presence of EDCI.

## Characterization

Identity of dyads and all new intermediates were confirmed by $^{1}$H NMR, and high resolution MS, and in the case of monomers, by $^{13}$C NMR. We did not obtain good quality $^{13}$C NMR spectra for dyads, due to the small quantity of sample and their sparse solubility.

Absorption and emission data for **NMP6-OMe** and **NMP7-OMe** were acquired in organic non-polar (toluene) and polar (N,N-dimethylformamide, DMF) solvents (Table 1). Fluorescence quantum yields ($\Phi_f$) of the bacteriochlorin components of dyads, where bacteriochlorin is directly excited (at $\lambda_{exc}$ = 515 nm and 530 nm, for **NMP6** and **NMP7**, respectively), corresponds well with that reported previously for analogous bacteriochlorin monomers in toluene.[24] In DMF however, the $\Phi_f$ of bacteriochlorin components in dyads is slightly reduced (1.25 fold for **NMP6** and 1.2-fold for **NMP7**), compared to that observed in toluene. This reduction of $\Phi_f$ is attributed to the competitive photoinduced electron transfer, which is facilitated in solvents of high dielectric constants. Energy transfer efficiency (ETE) was determined as a ratio of $\Phi_f$ of bacteriochlorin component when chlorin is selectively excited (at 419 nm, where bacteriochlorins possess negligible absorption) to the $\Phi_f$ when bacteriochlorin is directly excited, and was found to be 0.81–0.85 for **NMP6-OMe**, and 0.95–0.96 for **NMP7-OMe** (Table 1).

## Optical characteristics of hGSA-conjugated bacteriochlorin-based probes

The hGSA-probes target lectin receptors expressed on peritoneal ovarian cancer metastases (POCM).[3] Dequenching was measured by adding 1% odium Dodecyl Sulfate (SDS) to each probe. Since the absorbance spectra was identical before and after dequenching with 1% SDS, quenching was based on the FRET mechanism. No measurable spontaneous dequenching (~5%) of each probe was observed in mouse serum at 37 °C at 3 hours (h), demonstrating high *in vivo* stability (Figure 2, A: chlorin-bacteriochlorin dyads, B: BODIPY-bacteriochlorin dyads).

## *In vitro* fluorescent characterization of probes

Using fluorescence microscopy, minimal fluorescence was observed in targeted cells after 8 h of incubation with hGSA-conjugated bacteriochlorin-based probes. These signals were partially blocked by the addition of excess hGSA (Figure 2, A: chlorin-bacteriochlorin dyads, B: BODIPY-bacteriochlorin dyads).

### *In vivo* hGSA-based activatable imaging

To evaluate the feasibility of hGSA-conjugated bacteriochlorin probes for the detection of peritoneal metastases, each probe was injected into the peritoneal cavities of dsRedSHIN3 tumor bearing mice and the extracted bowel with its attached mesentery and images were obtained with a multispectral camera (Maestro). Fluorescence was spectrally unmixed to suppress background and identify chlorin-bacteriochlorin dyads (Figure 3A) and BODIPY-bacteriochlorin dyads (Figure 3B). The relative sensitivity of each probe was compared by imaging the specimen with the endogenous fluorophore transfected in the cell line (either green fluorescent protein, GFP or red fluorescent protein, RFP). Receiver Operating Characteristic (ROC) curves (true positive rate versus false positive rate) were generated and area under the curve (AUC) was determined. AUCs ranged between 0.85 and 0.95, indicating overall high accuracy that are excellent results (Figure 3).

### Optical characteristics of mAb-based activatable probes

Trastuzumab-conjugated NMP probes (tra-NMP6, tra-NMP7, tra-NMP11 and Tra-NMP12) or panitumumab-conjugated NMP probes (pan-NMP6, pan-NMP7, pan-NMP11 and pan-NMP12) were evaluated. The quenching capacities were measured by adding 1% SDS to dye-conjugated antibody (Figure 4). All antibody-conjugates were originally quenched but activated by adding SDS.

### *In vitro* fluorescent characterization of antibody-based probes

Each conjugate was evaluated by SDS-PAGE. In microscopic studies, minimal fluorescence signals were observed in targeted cells after overnight incubation with mAb-conjugated NMP probes. These signals were partially blocked by the addition of excess trastuzumab or panitumumab (Figure 5, A: chlorin-bacteriochlorin dyads, B: BODIPY-bacteriochlorin dyads)

### *In vivo* antibody-based activatable imaging

To evaluate the feasibility of trastuzumab-based activatable probes, we employed two types of murine cancer models, a GFP-transfected N87 gastric peritoneal metastasis model (intraperitoneal injection of probe) and a GFP transfected 3T3Her2 xenograft model (intravenous injection of probe). Multispectral imaging of the bowel-mesentery specimen was obtained and lesion sensitivity and specificity were compared with ROC analysis. The AUC of tra-NMP12 (0.9835) and tra-NMP11 (0.9578) were excellent (Figure 6). The AUCs of tra-NMP6 (0.5981) and tra-NMP7 (0.5674) (Figure 6) were poor. In a subcutaneously xenografted tumor-bearing mouse model, intravenous tra-NMP11 and tra-NMP12 both readily depicted HER2-positive tumors (Figure 7).

## DISCUSSION

Fluorescent probes are increasingly being used as adjuncts to open and endoscopic cancer surgery. The completeness of the surgical resection is strongly associated with longer survival of patients and the amount of residual tumor is a significant prognostic variable.[36–38] However, in complex tissues and organs it is possible to either miss or underestimate a specific cancer focus using visible white light imaging. A target-specific fluorescent agent

would be desirable to accurately identify such foci. PEGylated chlorin and BODIPY dyads of bacteriochlorin enable activatable and targetable probes offer promise in this area.[17, 18, 22, 39]

Bacteriochlorin derivatives have several advantages including narrow and tunable emission bands in the NIR region requiring only minor structural modifications.[19, 20, 22] Additionally, bacteriochlorin derivatives intrinsically have multiple absorbance spectra at visual and NIR ranges that allows us to perform *in vivo* fluorescence imaging at different depth.[19] The energy transfer dyads, chlorin-bacteriochlorin and BODIPY-bacteriochlorin, were developed to create NIR fluorophores with a common energy acceptor.[21, 22, 24] When these fluorophores were conjugated to targeting moieties, they became activatable imaging probes based on a FRET mechanism, a phenomenon that has been previously reported.[19, 20] We initially examined these compounds using hGSA as a targeting moiety and then used mAb for targeting. These targeting moieties were conjugated to four PEGylated bacteriochlorin-based dyads. These agents were then employed detecting peritoneal metastases in a disseminated gastric cancer model. This model generates a large number of small metastases in the mesentery which are labeled with GFP or RFP. This enables accurate determination of sensitivity and specificity for the experimental fluorescent agent.

We have previously reported successful NIR fluorescence imaging using non-PEGylated bacteriochlorin-based activatable probes which bound to ovarian cancer cells through the hGSA-lectin receptor interaction when intraperitoneally administered.[19, 20] hGSA is highly hydrophilic and the D-galactose receptor to which it binds is an optimal target for other peritoneal metastases models.[19, 20, 31, 32] However, since hGSA-based probes are quickly trapped by the liver after intravenous injection after the first pass, hGSA-based probes can be only be administered intraperitoneally, limiting applications. To enable broader applications of these fluorescent probes, mAb-conjugated probes would be highly desirable. However, bacteriochlorin-based fluorophores bound to mAb tend to aggregate and become insoluble. To address this issue we introduced bachteriochlorin-based dyads with PEG chains in order to decrease aggregation.

PEGylation is a well-established method to improve both *in vivo* pharmacokinetics and *in vivo* stability by conferring higher water solubility.[33–35] Although *in vitro* assays of mAb-based probes using chlorin-bacteriochlorin energy transfer dyads (NMP6 and NMP7) appeared hydrophilic, the fluorescence images in peritoneal cancer murine models were unsatisfactory probably because conjugation reaction with NMP6 and NMP7 altered the pharmacokinetics of antibody, resulted in insufficient delivery and activation of fluorescence signal. By exchanging the energy donor from chlorin to BODIPY, which possesses higher polarity and superior extinction coefficient in green light,[24] the BODIPY-bacteriochlorin energy transfer dyads (NMP11 and NMP12) were more efficient and therefore able to readily image the cancers with high sensitivity and specificity. (Figure 6 and Figure 7).

## CONCLUSION

In conclusion, we have developed new activatable mAb-bacteriochlorin-based NIR fluorescent probes that demonstrate high sensitivity for peritoneal metastases. The addition

of PEG chains to the bacteriochlorin improved hydrophilicity and reduced aggregation, leading to a viable *in vivo* imaging agent that detected cancer with high sensitivity in murine models. These fluorophores offer potential for multi-color fluorescence imaging and are a promising tool for precision medicine.

## MATERIALS AND METHODS

### General

Commercially available reagents and solvents were used without further purification. Commercially available anhydrous solvents were used for palladium-catalyzed reactions.

### General procedure for palladium cross-coupling reactions.

All reagents and solvents, with exception of palladium catalyst, were placed in a Schlenk flask and the contents were degassed by two cycles of freeze-pump-thaw. At which time the catalyst was added and a third cycle of free-pump-thaw was performed, and the reaction mixture was stirred under $N_2$ at indicated temperature.

### Microwave Reactions

Microwave reactions were performed in CEM Discover (CEM, Mathew, NC) microwave instrument. All reactions were performed in 10 mL closed tube, with continuous monitoring of pressure and temperature. Temperature was monitored using built-in IR sensor. The reaction cycle includes (1) irradiation of sample with 150 W for 2–3 minutes, upon which reaction temperature reaches 65–70 °C (2) 30 minutes “hold time” where reaction mixture was irradiated to keep the temperature at 65 °C, and (3) 10 minutes “cooling time” where reaction mixture was kept without irradiation in the closed vessel, until it reached temperature of about 50 °C.

### Characterization

All NMR spectra were acquired on either 400 MHz (Jeol) NMR or 500 MHz (Bruker) NMR. Note that for those compounds containing water soluble triazole-triethylene glycol monomethyl ether or triazole-tetraethylene glycol monomethyl ether, the corresponding (and highly overlapping) aliphatic signals exhibit slight over-integration during data processing. All HRMS data acquired on Bruker 12T FT-ICR MS.

### Spectroscopic Studies.

Fluorescence measurements were performed with sample absorbance of < 0.1. All measurements were performed in HPLC grade solvents.

Known compounds: THD-1,[40] DPM-1,[26] 3PEG-$N_3$,[28] 4PEG-$N_3$,[29] BC1,[23] BC2,[23] BC3,[23] as well as methyl esters of NMP11[23] and NMP12[23] were prepared following described procedures.

### Synthesis of Chlorin Monomers

**18,18-Dimethyl-3-bromo-10-(2,4,6-tripropar gyloxy)phenylchlorinato zinc(II) (ZnC1).—**Following the reported procedure,[26, 41] a solution of DPM-1 (1.05 g, 2.64 mmol)

in THF (26.4 mL) was treated with NBS (0.47 g, 2.6 mmol) at −78 °C. The resulting mixture was stirred at −78 °C for 45 min. The cooling bath was removed and hexane/water (40 mL 1:1) was added. The resulting mixture was extracted with ethyl acetate, organic phase was washed ($NH_4Cl$ and brine), dried ($Na_2SO_4$), and concentrated. The resulting crude product (1.28 g, 2.61 mmol) and THD-1 (701 mg, 2.61 mmol) in $CH_2Cl_2$ (78.3 mL) was treated with a solution of *p*-TsOH·$H_2O$ (2.98 g, 13.0 mmol) in methanol (26.1 mL) under nitrogen. The mixture was stirred for 30 min under nitrogen. The reaction mixture was then treated with 2,2,6,6-tetramethylpiperidine (13.3 mL, 78.1 mmol) and concentrated to dryness. The resulting brown solid was resuspended in acetonitrile (261 mL), and treated with 2,2,6,6-tetramethylpiperidine (13.3 mL, 78.1 mmol), $Zn(OAc)_2$ (7.17 g, 39.1 mmol), and AgOTf (2.01 g, 7.82 mmol). The resulting mixture was refluxed for 20 h exposed to air. The crude mixture was concentrated, filtered through a silica pad ($CH_2Cl_2$), collecting all blue-green material. The filtrate was chromatographed [silica, hexane/$CH_2Cl_2$ (1:10)]. The first blue-green fraction was identified as ZnC1 and the second one as ZnC2.

**ZnC1:** green powder, (293 mg, 16%). $^1$H NMR ($CDCl_3$, 500 MHz) δ 2.00 (s, 6H), 2.33 (t, *J* = 2.3 Hz, 2H), 2.71 (t, *J* = 2.4 Hz, 1H), 4.32–4.35 (m, 4H), 4.50 (s, 2H), 4.97 (d, *J* = 2.4 Hz, 2H), 6.86 (s, 2H), 8.48 (s, 1H), 8.53 (d, *J* = 4.2 Hz, 1H), 8.62 (d, *J* = 4.4 Hz, 1H), 8.67 (s, 1H) 8.71 (d, *J* = 4.4 Hz, 1H), 8.77 (s, 1H), 8.90 (d, *J* = 4.2 Hz, 1H), 9.74 (s, 1H); $^{13}$C NMR ($CDCl_3$, 125 MHz) δ 31.1, 45.4, 50.5, 56.8, 75.6, 76.2, 78.68, 78.70, 94.1, 94.9, 97.1, 107.5, 114.3, 115.2, 121.5, 127.3, 127.8, 128.6, 129.5, 133.1, 141.7, 146.2, 147.6, 149.0, 151.4, 153.8, 158.8, 159.3, 159.8, 170.5; HRMS (ESI-TOF) *m/z* $[M+H]^+$ Calcd for $C_{37}H_{28}BrN_4O_3Zn$ 718.05525; found 718.05610.

**ZnC2:** green powder (234 mg, 13%). $^1$H NMR ($CDCl_3$, 500 MHz) δ 1.99 (s, 3H), 2.00 (s, 3H), 2.30 (t, *J* = 2.3 Hz, 1H), 2.68 (t, *J* = 2.4 Hz, 1H), 4.34 (s, 2H), 4.50 (s, 2H), 4.84 (br s, 1H), 4.87 (d, *J* = 2.4 Hz, 2H), 6.52 (d, *J* = 2.3 Hz, 2H), 6.70 (d, *J* = 2.3 Hz, 2H), 8.49 (s, 1H), 8.54 (d, *J* = 4.0 Hz, 1H), 8.63 (d, *J* = 4.3 Hz, 1H), 8.67–8.70 (m, 2H), 8.75 (s, 1H), 8.90 (d, *J* = 4.1 Hz, 1H), 9.69 (s, 1H); $^{13}$C NMR ($CDCl_3$, 125 MHz) δ 31.07, 31.13, 45.5, 50.5, 56.39, 56.43, 75.6, 76.1, 78.6, 78.7, 94.3, 94.7, 95.0, 97.6, 107.6, 110.6, 111.8, 122.0, 127.8, 128.5, 128.6, 130.0, 132.7, 142.2, 146.7, 147.6, 148.3, 151.7, 154.0, 157.0, 158.4, 159.7, 160.4, 171.0; HRMS (ESI-TOF) *m/z* $[M+H]^+$ Calcd for $C_{34}H_{26}BrN_4O_3Zn$ 680.040005; found 680.39601.

**C3.—**In a 10 mL thick-walled glass tube, equipped with a magnetic stir-bar, samples of ZnC1 (50 mg, 0.069 mmol), 3PEG-$N_3$ (52.5 mg, 0.278 mmol), $CuSO_4$ (11.6 mg, 0.0485 mmol) and L-Ascorbic acid sodium salt (9.8 mg, 0.0495 mmol) were placed, and acetone (5 mL) and water (1 mL) were added. The tube was sealed with a septum and placed in the CEM microwave reactor. The reaction mixture was irradiated in a closed vessel with a pressure sensor, with 200 W power for 5 min, upon which the temperature of reaction mixture (monitored by IR sensor) reached 65 °C. The reaction mixture was kept in the microwave reactor at 65 ˚C for 30 min, upon which the complete consumption of the starting chlorin was confirmed by TLC (silica, $CH_2Cl_2$). The reaction mixture was allowed to cool down to room temperature and transferred into a round-bottomed-flask using the minimum amount of acetone and concentrated to dryness. The residue was dissolved in $CH_2Cl_2$ (5

mL), treated with a mixture of $CH_2Cl_2$ and TFA [20:1 (v/v)], and stirred at room temperature for 30 min. This reaction mixture was then poured slowly into an aqueous saturated sodium bicarbonate solution (approximately 150 mL). The organic layer was separated, and aqueous phase was extracted with $CH_2Cl_2$. Combined organic phase was washed with brine, dried (anhydrous $Na_2SO_4$), and concentrated. The residue was purified with silica column chromatography [$CH_2Cl_2$/MeOH (20:1)] to afford a green film (58 mg, 68%). $^1$H NMR ($CDCl_3$, 500 MHz) δ −2.16 (br s, 1H), −1.86 (br s, 1H), 2.04 (s, 6H), 2.36–2.43 (m, 4H), 2.49–2.55 (m, 4H), 2.64–2.69 (m, 4H), 2.86 (t, *J* = 4.6 Hz, 4H), 2.97 (s, 6H), 2.98–3.07 (m, 4H), 3.42 (s, 3H), 3.59–3.61 (m, 2H), 3.66–3.78 (m, 14H), 3.98 (t, *J* = 5.0 Hz, 2H), 4.61 (s, 2H), 4.68 (t, *J* = 5.0 Hz 2H), 5.01–5.08 (m, 4H), 5.47 (s, 2H), 6.00 (s, 2H), 6.88 (s, 2H), 8.10 (s, 1H), 8.54 (d, *J* = 4.3 Hz, 1H), 8.76–8.79 (m, 3H), 8.92 (d, *J* = 4.3 Hz, 1H), 8.97 (s, 1H), 8.98 (s, 1H), 9.86 (s, 1H); $^{13}$C NMR ($CDCl_3$, 125 MHz) δ 31.3, 46.4, 49.7, 50.6, 52.1, 58.7, 59.2, 62.5, 63.5, 68.6, 69.63, 69.68, 69.75, 69.81, 70.68, 70.72, 70.73, 70.76, 71.4, 72.1, 94.0, 94.5, 97.0, 105.2, 113.4, 113.9, 117.1, 123.0, 123.3, 124.5, 124.7, 128.9, 130.8, 132.0, 133.1, 137.0, 138.7, 140.2, 143.7, 143.9, 150.5, 155.0, 159.6, 160.9, 163.7, 175.0; HRMS (ESI-TOF) *m/z* $[M+H]^+$ Calcd for $C_{58}H_{75}BrN_{13}O_{12}$ 1224.48360; found 1224.48912.

**C4.—**Prepared in 83% yield (79 mg, 0.058 mmol) from C1 (50 mg, 0.070 mmol) according to the procedure described for C3. $^1$H NMR ($CDCl_3$, 400 MHz) δ −2.16 (br s, 1H), −1.86 (br s, 1H), 2.05 (s, 6H), 2.43–2.56 (m, 8H), 2.72–2.77 (m, 4H), 2.95 (t, *J* = 4.8 Hz, 4H), 2.97–3.05 (m, 4H), 3.01–3.18 (m, 16H), 3.39 (s, 3H), 3.55–3.58 (m, 2H), 3.66–3.71 (m, 12H), 3.73–3.78 (m, 4H), 3.99 (t, *J* =5.0 Hz, 2H), 4.61 (s, 2H), 4.68 (t, *J* =5.0 Hz, 2H), 5.01–5.08 (m, 4H), 5.47 (s, 2H), 6.00 (s, 2H), 6.89 (s, 2H), 8.09 (s, 1H), 8.54 (d, *J* = 4.3 Hz, 1H), 8.77–8.79 (m, 3H), 8.92 (d, *J* = 4.3 Hz, 1H), 8.97 (s, 2H), 9.86 (s, 1H); $^{13}$C NMR ($CDCl_3$, 125 MHz) δ 31.2, 46.3, 49.5, 50.5, 50.7, 58.8, 59.0, 62.4, 63.4, 68.5, 69.53, 69.59, 69.6, 69.8, 69.9, 70.00, 70.03, 70.5, 70.57, 70.58, 70.62, 70.64, 70.67, 70.69, 71.5, 71.95, 71.97, 93.9, 94.4, 96.9, 105.1, 113.2, 113.8, 116.9, 122.9, 123.2, 124.5, 128.8, 130.6, 131.9, 133.1, 136.9, 138.6, 140.0, 143.5, 143.7, 150.4, 154.9, 159.5, 160.8, 163.6, 174.9; HRMS (ESI-TOF) *m/z* $[M+Na]^+$ Calcd for $C_{64}H_{86}BrN_{13}O_{15}Na$ 1380.5440; found 1380.5458.

**C5.—**A mixture of C3 (32 mg, 0.026 mmol), 4-(methoxycarbonyl)phenylboronic acid pinacol ester (15.2 mg, 0.0580 mmol), $K_2CO_3$ (40.5 mg, 0.293 mmol), and $Pd(PPh_3)_4$ (3.6 mg, 0.0031 mmol) in toluene (6 mL) and DMF (3 mL) was degassed by following the general procedure, and was stirred at 80–90 ˚C under nitrogen. After 17 h, the mixture was diluted with ethyl acetate, washed (water and brine), dried ($Na_2SO_4$), and concentrated. The residue was purified with silica column chromatography [$CH_2Cl_2$/MeOH (20:1)] to afford a green film (27.4 mg, 82%). $^1$H NMR ($CDCl_3$, 500 MHz) δ −2.02 (s, 1H), −1.81 (br s, 1H), 2.08 (br s, 6H), 2.33–2.41 (m, 4H), 2.46–2.53 (m, 4H), 2.62–2.66 (m, 4H), 2.81–2.85 (m, 4H), 2.95 (s, 6H), 2.96–3.03 (m, 4H), 3.42 (s, 3H), 3.59–3.70 (m, 6H), 3.70–3.73 (m, 4H), 3.75 (t, *J* = 5.3 Hz, 4H), 3.99 (t, *J* = 5.1 Hz, 2H), 4.09 (s, 3H), 4.64 (s, 2H), 4.68 (t, *J* = 5.1 Hz, 2H), 5.01–5.06 (m, 4H), 5.47 (s, 2H), 6.00 (s, 2H), 6.88 (s, 2H), 8.10 (s, 1H), 8.41 (d, *J* = 8.2 Hz, 2H), 8.51 (d, *J* = 8.3 Hz, 2H), 8.54 (d, *J* = 4.2 Hz, 1H), 8.77 (s, 2H), 8.85 (d, *J* = 4.3 Hz, 1H), 8.91 (s, 1H), 8.98 (s 1H), 9.03 (s, 1H), 9.87 (s, 1H); $^{13}$C NMR ($CDCL_3$, 125 MHz) δ 31.4, 46.5, 49.7, 50.6, 52.2, 52.5, 58.9, 59.2, 62.5, 63.6, 68.6, 69.67, 69.73, 69.79,

70.73, 70.74, 70.78, 71.4, 72.1, 94.4, 94.6, 96.8, 106.3, 113.6, 121.4, 123.0, 124.2, 124.6, 128.7, 129.8, 130.6, 131.2, 131.3, 131.8, 133.2, 136.7, 138.6, 140.0, 140.1, 140.0, 143.7, 143.9, 150.9, 154.7, 159.6, 160.8, 163.5, 167.3, 174.9; HRMS (ESI-TOF) *m/z* $[M+H]^+$ Calcd for $C_{66}H_{82}N_{13}O_{14}$ 1280.61567; found 1280.60987.

**C6.—**Prepared in 76% yield (45 mg, 0.032 mmol) from C4 (60 mg, 0.044 mmol) according to the general procedure described for C5. $^1$H NMR ($CDCl_3$, 500 MHz) δ −1.99 (br s, 1H), −1.77 (br s, 1H), 2.08 (s, 6H), 2.46–2.55 (m, 8H), 2.74–2.77 (m, 4H), 2.95–2.97 (m, 4H), 2.97–3.04 (m, 4H), 3.12–3.17 (m, 22H), 3.39 (s, 3H), 3.55–3.58 (m, 2H), 3.66–3.70 (m, 12H), 3.74 (t, *J* = 5.3 Hz, 4H), 3.99 (t, *J* =5.2 Hz, 2H), 4.09 (s, 3H), 4.63 (s, 2H), 4.67 (t, *J* = 5.2 Hz, 2H), 5.02–5.07 (m, 4H), 5.48 (s, 2H), 6.01 (s, 2H), 6.91 (s, 2H), 8.08 (s, 1H), 8.41 (d, *J* = 8.3 Hz, 2H), 8.50 (d, *J* = 8.3 Hz, 2H), 8.56 (d, *J* = 4.3 Hz, 1H), 8.78 (s, 2H), 8.85 (d, *J* = 4.3 Hz, 1H), 8.91 (s, 1H), 8.97 (s, 1H), 9.03 (s, 1H), 9.87 (s, 1H); $^{13}$C NMR ($CDCl_3$, 125 MHz) δ 31.3, 46.4, 49.6, 50.6, 52.3, 52.4, 58.8, 59.1, 62.6, 63.6, 68.6, 69.6, 69.74, 69.76, 69.9, 70.0, 70.1, 70.67, 70.71, 70.78, 71.7, 72.1, 94.3, 94.7, 96.8, 106.2, 113.68, 113.73, 121.4, 122.9, 124.2, 124.5, 128.7, 129.8, 130.5, 131.18, 131.23, 131.8, 133.1, 136.7, 138.6, 140.0, 140.1, 140.8, 143.7, 143.9, 150.9, 154.8, 159.7, 160.9, 163.4, 167.2, 174.8; HRMS (ESI-TOF) *m/z* $[M+Na]^+$ Calcd for $C_{72}H_{93}N_{13}O_7Na$ 1434.6705; found 1434.6714.

## Synthesis of Bacteriochlorin-Chlorin Arrays

**NMP6-OMe.—**A mixture of C5 (10 mg, 0.0079 mmol), aqueous NaOH (1 mL, 3M), THF (1 mL), and methanol (1 mL) was stirred at room temperature for 1 h. An aqueous HCl solution (2 mL, 3M) was added, and resulting mixture was stirred for 5 minutes. The resulting mixture was extracted with $CH_2Cl_2$. Combined organic layers were washed with brine, dried ($Na_2SO_4$), and concentrated. The resulting crude acid (10 mg, 100%) was suspended in DMF (5 mL) and treated with DMAP (10.8 mg, 0.088 mmol), BC1 (5 mg, 0.0079 mmol), and EDCI (10.3 mg, 0.054 mmol). The resulting mixture was stirred at ambient temperature. After 19 h, the mixture was diluted with ethyl acetate, washed with brine, dried ($Na_2SO_4$), and concentrated. The residue was purified with silica column chromatography ($CH_2Cl_2$/MeOH (20:1)), followed by SEC column (THF) to afford a green film (2.9 mg, 20%). $^1$H NMR ($CDCl_3$, 400 MHz) δ −2.04 (bs s, 1H), −1.92 (br s, 1H), −1.78 (br s, 1H), −1.62 (br s, 1H), 1.99 (s, 6H), 2.01 (s, 6H), 2.11 (s, 6H), 2.46–2.49 (m, 4H), 2.56–2.60 (m, 4H), 2.72–2.75 (m, 4H), 2.90–2.93 (m, 4H), 3.00 (s, 6H), 3.02–3.05 (m, 4H), 3.43 (s, 3H), 3.59–3.7 (m, 14H), 3.79 (s, 3H), 3.96–4.00 (m, 2H), 4.07 (s, 3H), 4.42 (s, 2H), 4.45 (s, 2H), 4.65–4.70 (m, 4H), 5.04–5.11 (m, 4H), 5.49 (s, 2H), 6.06 (s, 2H), 6.91 (s, 2H), 8.10–8.13 (m, 3H), 8.25 (d, *J* = 8.5 Hz, 2H), 8.29 (d, *J* = 8.5 Hz, 2H), 8.33 (s, 3H), 8.43 (d, *J* = 8.4 Hz, 2H), 8.51 (s, 1H), 8.59 (d, *J* = 4.3 Hz, 1H), 8.68–8.72 (m, 3H), 8.78–8.83 (m, 4H), 8.84 (d, *J* = 2.1 Hz, 1H), 8.90 (d, *J* = 4.3 Hz, 1H), 8.93 (s, 1H), 8.95 (s, 1H), 8.99 (s, 1H), 9.84 (s, 1H); HRMS (ESI-TOF) *m/z* $[M+Na]^+$ Calcd for $C_{104}H_{116}N_{18}O_{16}Na$ 1895.8709; found 1895.8766.

**NMP7-OMe.—**A mixture of BC3 (16.4 mg, 18.1 mmol), C4 (27.1 mg, 20.0 mmol), $Na_2CO_3$ (19.1 mg, 181 mmol), $PdCl_2(dppf)\cdot CH_2Cl_2$ (7.4 mg, 9.1 mmol), was dissolved in toluene/EtOH/$H_2O$ (4:1:2), degassed following the general procedure for freeze-pump-thaw and stirred under $N_2$ for 14 hours. TLC indicated complete consumption of starting materials

at that time. Reaction mixture was diluted with $CH_2Cl_2$ and washed with water, brine, then dried ($Na_2SO_4$) and concentrated. The dark maroon-purple residue was purified by gravity column chromatography [silica, $CH_2Cl_2$/MeOH (1:0) → (40:1) → (30:1) → (20:1)], yielding a purple solid (4.4 mg, 12%). $^1$H NMR ($CDCl_3$, 400 MHz) δ −2.02 (s, 1H), −1.79 (s, 1H), −1.76 (s, 1H), −1.52 (s, 1H), 1.97 (s, 6H), 1.98 (s, 6H), 2.54–2.63 (m, 8H), 2.82–2.86 (m, 4H), 3.17 (s, 6H), 3.19–3.22 (m, 9H), 3.39 (s, 3H), 3.56–3.59 (m 2H), 3.64–3.79 (m, 20H) 4.00 (s, 3H), 4.45 (s, 2H), 4.48 (s, 2H), 4.55 (s, 3H), 4.65 (s, 2H), 4.69 (t, $J$ = 5.0 Hz, 2H), 5.03–5.10 (m, 4H), 5.48 (s, 2H), 6.02 (s, 2H), 6.90 (s, 2H), 7.92–7.99 (m, 5H), 8.10 (s, 1H), 8.19 (d, $J$ =8.3 Hz, 2H), 8.34–8.43 (m, 3H), 8.56–8.60 (m, 4H), 8.78–8.85 (m, 3H), 8.87 (d, $J$ = 4.3 Hz, 1H), 8.99–9.01 (m, 2H), 9.86 (s, 1H).

## Synthesis of Bioconjugatable Bacteriochlorin-chlorin arrays

Bioconjugatable arrays NMP6 and NMP7 were prepared by hydrolysis of methyl esters NMP6-OMe and NMP7-OMe, respectively, followed by EDC coupling with N-hydroxysuccinimide.

Hydrolysis step was performed by dissolving dyad sample, either NMP6-OMe or NMP7-OMe (5.0 mmol) in 3 mL THF/MeOH (2:1) and treating with 1 mL 2M NaOH, vigorously stirring for 1.5 hours, monitoring progress by TLC. Once deemed complete, the reaction mixture was acidified with 5% HCl (aq.), washed with brine, dried ($Na_2SO_4$) and concentrated. Crude residue of dyad-acid intermediate was checked for structural integrity by absorption and emission spectroscopy.

Dyad acid intermediate was then dissolved in 1 mL of DMF and treated with DMAP (20 mmol), EDC·HCl (20 mmol), and N-hydroxysuccinimide (50 mmol) and stirred vigorously overnight. Reaction progress was monitored by TLC and deemed complete at 24 hours. Reaction mixture was then diluted with $CH_2Cl_2$, washed with water, brine, dried ($Na_2SO_4$) and concentrated to dryness. Both arrays appear as a purple solid and were obtained in ~50% yield (~5 mg) after the two above described steps. Due to low quantities, we were unable to acquire high-quality NMR data, and the integrity of dyads was determined by absorption and emission spectra, which are identical with those of methyl ester.

## Synthesis of Bacteriochlorin-BODIPY arrays

**NMP11:** A sample of corresponding methyl ester (20.2 mg, 10.6 μmol) was dissolved in THF/MeOH (2:1, 3 mL) and treated with 2 M NaOH (1 mL). Mixture was stirred at room temperature for one hour, then diluted with EtOAc, washed with water, then acidified (5% HCl), washed with brine, dried ($Na_2SO_4$) and concentrated. Intermediate carboxylic acid was a purple solid upon concentration and drying. Intermediate integrity was confirmed by absorption spectrum and HRMS [(ESI-TOF) $m/z$ $[M+Na]^+$ Calcd for $C_{100}H_{121}BF_2N_{16}O_{19}Na$ 1922.8987; found 1922.8930]. Dyad carboxylic acid intermediate (12.5 mg, 6.58 μmol), DMAP (3.2 mg, 26.3 μmol), and EDC·HCl (5.1 mg, 26.3 μmol) were dissolved in DMF (1 mL), treated with N-hydroxysuccinimide (7.6 mg, 65.8 μmol), then stirred at room temperature. After 24 hours, the reaction was diluted with EtOAc, washed with water, brine, dried ($Na_2SO_4$) and concentrated. Product was yielded as a purple solid (11.3 mg, 86%). Absorption and emission spectra (in DMF) are identical with those of

methyl ester, confirming integrity of array. HRMS (ESI-TOF) *m/z* $[M+Na]^+$ Calcd for $C_{104}H_{124}BF_2N_{17}O_{21}Na$ 2019.9150; found 2019.9087.

**NMP12:** A sample of corresponding methyl ester (20.1 mg, 10.2 μmol) was dissolved in THF/MeOH (2:1, 3 mL) and treated with 2 M NaOH (1 mL). Mixture was stirred at room temperature for one hour, then diluted with EtOAc, washed with water, then acidified (5% HCl), washed with brine, dried ($Na_2SO_4$) and concentrated. Carboxylic acid intermediate was yielded as a purple solid, and identity confirmed by HRMS [(ESI-TOF) *m/z* $[M+Na]^+$ Calcd for $C_{104}H_{121}BF_2N_{16}O_{19}Na$ 1970.8987; found 1970.8944]. Dyad carboxylic acid intermediate (15.2 mg, 7.80 μmol), DMAP (3.2 mg, 31.2 μmol), and EDC·HCl (6.0 mg, 31.2 μmol) were dissolved in DMF (1 mL), treated with N-hydroxysuccinimide (9.0 mg, 78.0 μmol), and stirred at room temperature. After 24 hours, the reaction was diluted with EtOAc, washed with water, brine, dried ($Na_2SO_4$) and concentrated. Product was yielded as a purple solid (11.3 mg, 86%). Absorption and emission spectra (in DMF) are identical with those of methyl ester, confirming integrity of array. HRMS (ESI-TOF) *m/z* $[M+Na]^+$ Calcd for $C_{108}H_{124}BF_2N_{17}O_{21}Na$ 2067.9151; found 2067.9049.

## Synthesis, Chemical Activation, and Stability in Serum of hGSA-NMP Conjugates and mAb-NMP Conjugates

The synthesis methods of chlorin-bacteriochlorin energy-transfer dyads, NMP6 and NMP7, and BODIPY bacteriochlorin energy-transfer dyads, NMP11 and NMP12, have been published.[22, 24] hGSA was incubated with each NMP-NHS ester at a ratio of 1:5 in 0.1 M Na2HPO4 (pH8.6) at room temperature for 1 h, followed by purification with a size exclusion column (PD-10; GE Healthcare, Piscataway, NJ). The NMP labeling mAb was also produced by reacting mAb with each NMP at a ratio of 1:10, respectively, in the same manner as hGSA-NMP conjugates. The protein concentration was also determined by measuring the absorption at 280 nm with the UV−vis system. The number of fluorophore molecules conjugated with each hGSA molecule was confirmed by dividing the dye concentration by the protein concentration. The quenching abilities of each conjugate were investigated by denaturing each with 1% SDS as described previously.[5, 42] Briefly, the conjugates were incubated with either 1% SDS in PBS or PBS for 15 min at room temperature. The change in fluorescence intensity of each conjugate was investigated with an *in vivo* imaging system (Maestro, CRi Inc., Woburn, MA) using the following filter set: 503−555 nm for excitation light and long-pass filter over 700 nm for emission light. Each probe was added to mouse serum and the serum samples were incubated at 37 °C for 0, 1, 2, and 3 h. After incubation, the change in fluorescence intensity was evaluated with a Maestro camera. We also performed sodium dodecyl sulfate polyacrylamide gel electrophoresis (SDS-PAGE). The conjugate was separated by SDS-PAGE with a 4%–20% gradient polyacrylamide gel (Life Technologies). A standard marker (Crystalgen Inc.) was used as a protein molecular weight marker. After electrophoresis at 80 V for 2.5 h, the gel was imaged with the Maestro system (CRI, Woburn, MA) using spectral imaging. We used diluted trastuzumab or panitumumab with the probe as a control. The gel was stained with Colloidal Blue Staining kit to determine the molecular weight of the conjugate.

## Cell Culture

The established ovarian cancer cell line, DsRedSHIN3, was used for *in vitro* fluorescence microscopic analysis and *in vivo* optical imaging of POCM. DsRedSHIN3 cells express the red fluorescent protein (RFP DsRed2)- and served as the standard of reference for cancer detection.[43] HER2-expressing 3T3 cells, which are human fibroblast cells, and EGFR-expressing, MDA-MB468 cells, which are human breast cancer cells, and N87-GFP cells, which are human gastric cancer cells were used as target cells for mAb-conjugated NMP probes Cells were grown in RPMI 1640 medium (Invitrogen) containing 10% fetal bovine serum (Gibco), 0.03% L-glutamine, 100 U/mL penicillin, and 100 μg/mL streptomycin at 37 °C, 5% $CO_2$.

## Flow Cytometry

Flow cytometry of cells labeled with NMP probes was performed (FACS Calibur, BD BioSciences, San Jose, CA, USA) using CellQuest software (BD BioSciences). Cells ($5\times10^4$) were incubated with each NMP probe overnight at 37°C. Propidium iodide - positive dead cells were gated out, and the remaining cells were subjected to further analyses. To validate the specific binding of the conjugated antibody, excess antibody (50 μg, trastuzumab or panitumumab) was added 1 h before the addition of probes to block 0.5 μg of the probe.

## Fluorescence Microscopic Studies

SHIN3 cells ($5\times10^4$) for hGSA-NMP probes or MDA-MB468 cells and N87 cells ($5\times10^4$) for mAb-NMP probes were plated on a cover glass bottomed culture well and incubated for 16 h. Each probe was then added at 1 μg/mL. The cells were incubated for either 8 h for hGSA-NMP probes or overnight for mAb-NMP probes followed by washing once with PBS, and fluorescence microscopic analysis was performed using an Olympus BX61 microscope (Olympus America, Inc., Melville, NY) equipped with the following filters: excitation wavelength 380−420 nm and emission wavelength range 700 nm longpass. Transmitted light differential interference contrast (DIC) images were obtained as well. To validate the specific binding of the probe, 100 μg of non-conjugated hGSA was added to block 1 μg of conjugate 2 h before incubation of the probe.

## Animal Model of Peritoneal Metastases

All procedures were carried out in compliance with the Guide for the Care and Use of Laboratory Animal Resources (1996), US National Research Council, and were approved by the local Animal Care and Use Committee. Six to eight-week-old female homozygote athymic nude mice were purchased from Charles River (National Cancer Institute, Frederick, MD). Two groups of intraperitoneal xenografts were established by intraperitoneal.injection of $2\times10^6$ SHIN3 DsRed cells for hGSA-NMP probes and $1\times10^6$ N87-GFP cells for mAb-NMP probes suspended in 300 μL of PBS into the peritoneal cavity of nude mice. Imaging was performed 14−21 days after injection of the cells.

### *In Vivo* Activatable Imaging of Peritoneal Metastases after Peritoneal Injection of Probes

The hGSA-NMP probes (each 25 μg) were injected into the peritoneal cavities of SHIN3 DsRed (RFP) tumor bearing mice (n = 5 in each group). The tra-NMP probes (each 100 μg) were intraperitoneally administered to N87-GFP tumor bearing mice (n = 4 in each group) Mice were euthanized by carbon dioxide inhalation after 1 h for hGSA-NMP probes injection or 1 day for mAb-NMP probes. After euthanasia, the mouse abdominal wall was incised, and the abdominal cavity was exposed. The bowel and mesentery were extracted, and close-up images were obtained. Spectral fluorescence images were acquired using the Maestro In-Vivo Imaging System. The following filter set was used for imaging each NMP probes, RFP for hGSA-NMP probes, and GFP for mAb-NMP probes: a band-pass filter from 503 to 555 nm for excitation light and a long-pass filter over 700 nm for emission light for NMP probes, a long-pass filter over 580 nm for emission for RFP and GFP. The tunable emission filter was automatically stepped in 10 nm increments at constant exposure to generate a spectral image. The spectral fluorescence images consist of auto-fluorescence spectra and the spectra from each NMP probe and RFP or GFP, which were then unmixed, based on their spectral patterns using commercial software (Maestro software; CRi). Spectrally resolved RFP or GFP images, NMP probe images, and composite images were obtained.

### Assessment of Sensitivity and Specificity of NMP Probes in the Detection of Peritoneal Metastases

Sensitivity and specificity were determined by comparing sites of fluorescence from the hGSA-NMP probe with sites of fluorescence from RFP-transfected SHIN3 tumors. The spectral fluorescence images were unmixed, and regions of interest (ROI) were assigned using automated software based on a predetermined threshold. Only nodules with short axis diameters >0.5 mm were included for analysis. RFP-positive nodules were defined as having an average fluorescence intensity >20 a.u. on images unmixed for the RFP spectra. True positives for the hGSA-NMP probe were defined as ROIs with an average fluorescence intensity of >5 a.u, whereas true negatives for hGSA-NMP4 and hGSA-NMP5 were defined as ROIs with an average fluorescence intensity <5 a.u. on the spectrally unmixed images. False positives for the hGSA-NMP probe were defined as ROIs in which fluorescence was seen only on the NMP probes image and not on the RFP image.

### *In Vivo* Activatable Imaging of Tumors after Intravenous Injection of Mab-NMP Probes

Tumor models were established by injecting five million 3T3Her2-GFP cells subcutaneously in the right dorsum of the mice. The tra-NMP probes (each 200 μg) was intravenously administered to N87-GFP tumor bearing mice (n = 3 in each group). Mice were euthanized by carbon dioxide the next day. After euthanasia, spectral fluorescence images were acquired using the Maestro In-Vivo Imaging System of the bowel and mesentery. The following filter set was used for imaging each NMP probe and GFP: a band-pass filter from 503 to 555 nm for excitation light and a long-pass filter over 700 nm for emission light for NMP probes, a long-pass filter over 580 nm for emission for GFP. The spectral fluorescence images consist of auto-fluorescence spectra and the spectra from each NMP probe and GFP, which were then unmixed, based on their spectral patterns using commercial software

(Maestro software; CRi). Spectrally resolved GFP images, NMP probe images, and composite images were made.

### Statistical Analysis

The accuracy of the NMP probes in identifying target cells was evaluated by calculating the areas under a ROC curve.[44] The AUC results were considered excellent for AUC values between 0.9-and 1.0, good for AUC values between 0.8 and-0.9, fair for AUC values between 0.7-and 0.8, poor for AUC values below −0.7.[45–47] All analyses were performed using a GraphPad Prism 6 package (GraphPad, La Jolla, CA).

## ACKNOWLEDGEMENTS

This research was supported by the Intramural Research Program of the National Institutes of Health, National Cancer Institute, Center for Cancer Research (ZIA-BC011512) and the National Cancer Institute of the National Institutes of Health under Award Number U01CA181628 (to M.P.). The content is solely the responsibility of the authors and does not necessarily represent the official views of the National Institutes of Health. We thank Mr. Nopondo N. Esemoto, for synthesis of compound **C6**.

## ABBREVIATIONS

| | |
|---|---|
| **mAb** | Monoclonal antibody |
| **NIR** | Near infrared |
| **BODIPY** | boron-dipyrromethene |
| **PEG** | polyethylene glycol |
| **TBR** | tumor to background ratio |
| **FRET** | Förster resonance energy transfer |
| **PeT** | photo-induced energy transfer |
| **MMP-2** | matrix metalloproteinases-2 |
| **Cy** | cyanine dye |
| **ICG** | indocyanine green dyes |
| **hGSA** | galactosyl-human serum albumin |
| **DMF** | N,N-dimethylformamide |
| **SDS** | odium Dodecyl Sulfate |
| **ETE** | Energy transfer efficiency |
| **POCM** | peritoneal ovarian cancer metastases |
| **h** | hours |
| **GFP** | green fluorescent protein |

| | |
|---|---|
| **RFP** | red fluorescent protein |
| **ROC** | Receiver Operating Characteristic |
| **AUC** | area under the curve |
| **SEM** | standard error of the mean |

## REFERENCES


(1). Weissleder R, and Mahmood U (2001) Molecular imaging. Radiology 219, 316–333. [PubMed: 11323453]

(2). Weissleder R, and Pittet MJ (2008) Imaging in the era of molecular oncology. Nature 452, 580–589. [PubMed: 18385732]

(3). Kobayashi H, Ogawa M, Alford R, Choyke PL, and Urano Y (2010) New strategies for fluorescent probe design in medical diagnostic imaging. Chem Rev 110, 2620–2640. [PubMed: 20000749]

(4). Kobayashi H, Longmire MR, Ogawa M, and Choyke PL (2011) Rational chemical design of the next generation of molecular imaging probes based on physics and biology: mixing modalities, colors and signals. Chem Soc Rev 40, 4626–4648. [PubMed: 21607237]

(5). Ogawa M, Kosaka N, Choyke PL, and Kobayashi H (2009) In vivo molecular imaging of cancer with a quenching near-infrared fluorescent probe using conjugates of monoclonal antibodies and indocyanine green. Cancer Res 69, 1268–1272. [PubMed: 19176373]

(6). Alford R, Ogawa M, Hassan M, Gandjbakhche AH, Choyke PL, and Kobayashi H (2010) Fluorescence lifetime imaging of activatable target specific molecular probes. Contrast Media Mol Imaging 5, 1–8. [PubMed: 20101762]

(7). Kobayashi H, and Choyke PL (2011) Target-cancer-cell-specific activatable fluorescence imaging probes: rational design and in vivo applications. Acc Chem Res 44, 83–90. [PubMed: 21062101]

(8). Savariar EN, Felsen CN, Nashi N, Jiang T, Ellies LG, Steinbach P, Tsien RY, and Nguyen QT (2013) Real-time in vivo molecular detection of primary tumors and metastases with ratiometric activatable cell-penetrating peptides. Cancer Res 73, 855–864. [PubMed: 23188503]

(9). Whitley MJ, Cardona DM, Lazarides AL, Spasojevic I, Ferrer JM, Cahill J, Lee CL, Snuderl M, Blazer DG 3rd, Hwang ES, et al. (2016) A mouse-human phase 1 co-clinical trial of a protease-activated fluorescent probe for imaging cancer. Sci Transl Med 8, 320ra324.

(10). Miampamba M, Liu J, Harootunian A, Gale AJ, Baird S, Chen SL, Nguyen QT, Tsien RY, and Gonzalez JE (2017) Sensitive in vivo Visualization of Breast Cancer Using Ratiometric Protease-activatable Fluorescent Imaging Agent, AVB-620. Theranostics 7, 3369–3386. [PubMed: 28900516]

(11). Tung CH, Bredow S, Mahmood U, and Weissleder R (1999) Preparation of a cathepsin D sensitive near-infrared fluorescence probe for imaging. Bioconjug Chem 10, 892–896. [PubMed: 10502358]

(12). Tung CH, Mahmood U, Bredow S, and Weissleder R (2000) In vivo imaging of proteolytic enzyme activity using a novel molecular reporter. Cancer Res 60, 4953–4958. [PubMed: 10987312]

(13). Bremer C, Bredow S, Mahmood U, Weissleder R, and Tung CH (2001) Optical imaging of matrix metalloproteinase-2 activity in tumors: feasibility study in a mouse model. Radiology 221, 523–529. [PubMed: 11687699]

(14). Lebel R, and Lepage M (2014) A comprehensive review on controls in molecular imaging: lessons from MMP-2 imaging. Contrast Media Mol Imaging 9, 187–210. [PubMed: 24700747]

(15). Licha K, and Olbrich C (2005) Optical imaging in drug discovery and diagnostic applications. Adv Drug Deliv Rev 57, 1087–1108. [PubMed: 15908041]

(16). Cao W, Ng KK, Corbin I, Zhang Z, Ding L, Chen J, and Zheng G (2009) Synthesis and evaluation of a stable bacteriochlorophyll-analog and its incorporation into high-density lipoprotein nanoparticles for tumor imaging. Bioconjug Chem 20, 2023–2031. [PubMed: 19839633]

(17). Liu TW, Chen J, Burgess L, Cao W, Shi J, Wilson BC, and Zheng G (2011) Multimodal bacteriochlorophyll theranostic agent. Theranostics 1, 354–362. [PubMed: 21938263]

(18). Lovell JF, Jin CS, Huynh E, Jin H, Kim C, Rubinstein JL, Chan WC, Cao W, Wang LV, and Zheng G (2011) Porphysome nanovesicles generated by porphyrin bilayers for use as multimodal biophotonic contrast agents. Nat Mater 10, 324–332. [PubMed: 21423187]

(19). Alexander VM, Sano K, Yu Z, Nakajima T, Choyke PL, Ptaszek M, and Kobayashi H (2012) Galactosyl human serum albumin-NMP1 conjugate: a near infrared (NIR)-activatable fluorescence imaging agent to detect peritoneal ovarian cancer metastases. Bioconjug Chem 23, 1671–1679. [PubMed: 22799539]

(20). Harada T, Sano K, Sato K, Watanabe R, Yu Z, Hanaoka H, Nakajima T, Choyke PL, Ptaszek M, and Kobayashi H (2014) Activatable organic near-infrared fluorescent probes based on a bacteriochlorin platform: synthesis and multicolor in vivo imaging with a single excitation. Bioconjug Chem 25, 362–369. [PubMed: 24450401]

(21). Kee HL, Nothdurft R, Muthiah C, Diers JR, Fan D, Ptaszek M, Bocian DF, Lindsey JS, Culver JP, and Holten D (2008) Examination of chlorin-bacteriochlorin energy-transfer dyads as prototypes for near-infrared molecular imaging probes. Photochem Photobiol 84, 1061–1072. [PubMed: 18673324]

(22). Yu Z, and Ptaszek M (2013) Near-IR emissive chlorin-bacteriochlorin energy-transfer dyads with a common donor and acceptors with tunable emission wavelength. J Org Chem 78, 10678–10691. [PubMed: 24079536]

(23). Meares A, Satraitis A, Akhigbe J, Santhanam N, Swaminathan S, Ehudin M, and Ptaszek M (2017) Amphiphilic BODIPY-Hydroporphyrin Energy Transfer Arrays with Broadly Tunable Absorption and Deep Red/Near-Infrared Emission in Aqueous Micelles. J Org Chem 82, 6054–6070. [PubMed: 28516773]

(24). Meares A, Satraitis A, and Ptaszek M (2017) BODIPY-Bacteriochlorin Energy Transfer Arrays: Toward Near-IR Emitters with Broadly Tunable, Multiple Absorption Bands. J Org Chem 82, 13068–13075. [PubMed: 29119786]

(25). Yang E, Kirmaier C, Krayer M, Taniguchi M, Kim HJ, Diers JR, Bocian DF, Lindsey JS, and Holten D (2011) Photophysical properties and electronic structure of stable, tunable synthetic bacteriochlorins: extending the features of native photosynthetic pigments. J Phys Chem B 115, 10801–10816. [PubMed: 21875047]

(26). Liu M, Chen CY, Mandal AK, Chandrashaker V, Evans-Storms RB, Pitner JB, Bocian DF, Holten D, and Lindsey JS (2016) Bioconjugatable, PEGylated Hydroporphyrins for Photochemistry and Photomedicine. Narrow-Band, Red-Emitting Chlorins. New J Chem 40, 7721–7740.

(27). El-Faham A, and Albericio F (2011) Peptide coupling reagents, more than a letter soup. Chem Rev 111, 6557–6602. [PubMed: 21866984]

(28). Dan K, Bose N, and Ghosh S (2011) Vesicular assembly and thermo-responsive vesicle-to-micelle transition from an amphiphilic random copolymer. Chem Commun (Camb) 47, 12491–12493. [PubMed: 22020054]

(29). Li G, Bhosale SV, Wang T, Hackbarth S, Roeder B, Siggel U, and Fuhrhop JH (2003) Nanowells on silica particles in water containing long-distance porphyrin heterodimers. J Am Chem Soc 125, 10693–10702. [PubMed: 12940755]

(30). Vegesna GK, Sripathi SR, Zhang J, Zhu S, He W, Luo FT, Jahng WJ, Frost M, and Liu H (2013) Highly water-soluble BODIPY-based fluorescent probe for sensitive and selective detection of nitric oxide in living cells. ACS Appl Mater Interfaces 5, 4107–4112. [PubMed: 23614822]

(31). Hama Y, Urano Y, Koyama Y, Choyke PL, and Kobayashi H (2006) Targeted optical imaging of cancer cells using lectin-binding BODIPY conjugated avidin. Biochemical and Biophysical Research Communications 348, 807–813. [PubMed: 16904640]

(32). Hama Y, Urano Y, Koyama Y, Gunn AJ, Choyke PL, and Kobayashi H (2007) A self-quenched galactosamine-serum albumin-rhodamineX conjugate: a “smart” fluorescent molecular imaging probe synthesized with clinically applicable material for detecting peritoneal ovarian cancer metastases. Clin Cancer Res 13, 6335–6343. [PubMed: 17975145]

(33). Caliceti P, and Veronese FM (2003) Pharmacokinetic and biodistribution properties of poly(ethylene glycol)-protein conjugates. Adv Drug Deliv Rev 55, 1261–1277. [PubMed: 14499706]

(34). Jokerst JV, Lobovkina T, Zare RN, and Gambhir SS (2011) Nanoparticle PEGylation for imaging and therapy. Nanomedicine (Lond) 6, 715–728. [PubMed: 21718180]

(35). Sano K, Nakajima T, Miyazaki K, Ohuchi Y, Ikegami T, Choyke PL, and Kobayashi H (2013) Short PEG-Linkers Improve the Performance of Targeted, Activatable Monoclonal Antibody-Indocyanine Green Optical Imaging Probes. Bioconjug Chem 24, 811–816. [PubMed: 23600922]

(36). Bristow RE, and Berek JS (2006) Surgery for ovarian cancer: how to improve survival. Lancet 367, 1558–1560. [PubMed: 16698396]

(37). Vergote I, Trope CG, Amant F, Kristensen GB, Ehlen T, Johnson N, Verheijen RH, van der Burg ME, Lacave AJ, Panici PB, et al. (2010) Neoadjuvant chemotherapy or primary surgery in stage IIIC or IV ovarian cancer. N Engl J Med 363, 943–953. [PubMed: 20818904]

(38). Hoogstins CE, Tummers QR, Gaarenstroom KN, de Kroon CD, Trimbos JB, Bosse T, Smit VT, Vuyk J, van de Velde CJ, Cohen AF, et al. (2016) A Novel Tumor-Specific Agent for Intraoperative Near-Infrared Fluorescence Imaging: A Translational Study in Healthy Volunteers and Patients with Ovarian Cancer. Clin Cancer Res 22, 2929–2938. [PubMed: 27306792]

(39). Alford R, Simpson HM, Duberman J, Hill GC, Ogawa M, Regino C, Kobayashi H, and Choyke PL (2009) Toxicity of organic fluorophores used in molecular imaging: literature review. Mol Imaging 8, 341–354. [PubMed: 20003892]

(40). Ptaszek M, Bhaumik J, Kim HJ, Taniguchi M, and Lindsey JS (2005) Refined Synthesis of 2,3,4,5-Tetrahydro-1,3,3-trimethyldipyrrin, a Deceptively Simple Precursor to Hydroporphyrins. Org Process Res Dev 9, 651–659. [PubMed: 19132135]

(41). Ptaszek M, Lahaye D, Krayer M, Muthiah C, and Lindsey JS (2010) De novo synthesis of long-wavelength absorbing chlorin-13,15-dicarboximides. J Org Chem 75, 1659–1673. [PubMed: 20121051]

(42). Ogawa M, Kosaka N, Choyke PL, and Kobayashi H (2009) H-type dimer formation of fluorophores: a mechanism for activatable, in vivo optical molecular imaging. ACS Chem Biol 4, 535–546. [PubMed: 19480464]

(43). Hama Y, Urano Y, Koyama Y, Choyke PL, and Kobayashi H (2007) D-galactose receptor-targeted in vivo spectral fluorescence imaging of peritoneal metastasis using galactosamin-conjugated serum albumin-rhodamine green. J Biomed Opt 12, 051501. [PubMed: 17994865]

(44). Hanley JA, and McNeil BJ (1982) The meaning and use of the area under a receiver operating characteristic (ROC) curve. Radiology 143, 29–36. [PubMed: 7063747]

(45). Obuchowski NA (2003) Receiver operating characteristic curves and their use in radiology. Radiology 229, 3–8. [PubMed: 14519861]

(46). Ludemann L, Grieger W, Wurm R, Wust P, and Zimmer C (2006) Glioma assessment using quantitative blood volume maps generated by T1-weighted dynamic contrast-enhanced magnetic resonance imaging: a receiver operating characteristic study. Acta Radiol 47, 303–310. [PubMed: 16613313]

(47). El Khouli RH, Macura KJ, Barker PB, Habba MR, Jacobs MA, and Bluemke DA (2009) Relationship of temporal resolution to diagnostic performance for dynamic contrast enhanced MRI of the breast. J Magn Reson Imaging 30, 999–1004. [PubMed: 19856413]

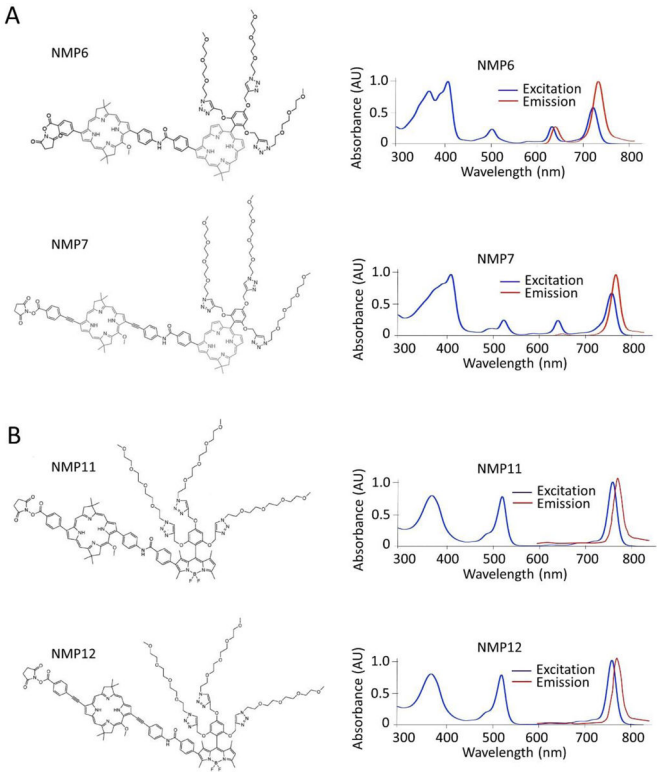


**Figure 1.**

Chemical structures and spectral profiles of Chlorin-Bacteriochlorin dyads, NMP6 and NMP7 (A), and BODIPY-Bacteriochlorin dyads, NMP11 and NMP12 (B). They were all conjugated by NHS ester and modified by multiple PEGylation. They have multiple available excitation (blue) bands and yield an NIR emission (red). The emission wavelength of NMP7 (770 nm) is longer than that of NMP6 (748 nm). The same applies to NMP12 (770 nm) and NMP11 (746 nm).

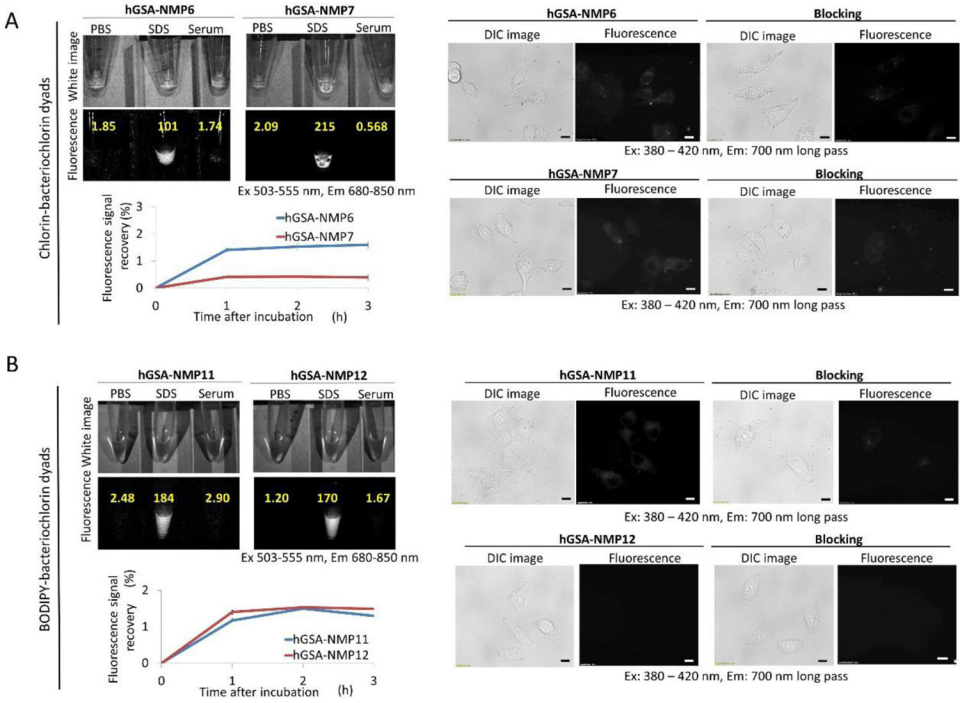


**Figure 2.**

Fluorescence quenching properties and stability in serum (left) and *in vitro* imaging of SHIN3 cells (right) of hGSA-NMP6, hGSA-NMP7 (A) and hGSA-NMP11, hGSA-NMP12 (B). No measurable dequenching of the four types of hGSA-conjugates probes was observed in mouse serum at 37 ˚C for 3 hrs. Fluorescence recovery was caluculated by the following equation: (fluorescence signal in mouse serum − fluorescence signal in PBS)/(fluorescence signal in SDS/PBS − fluorescence signal in PBS) × 100. Data are presented as mean ± SEM. Each probe exhibited high stability in mouse serum for 3 h. Microscope images obtained after the overnight incubation of the probes. To validate the specific binding of the probes, excess hGSA was used 2 h before incubation of the probes.

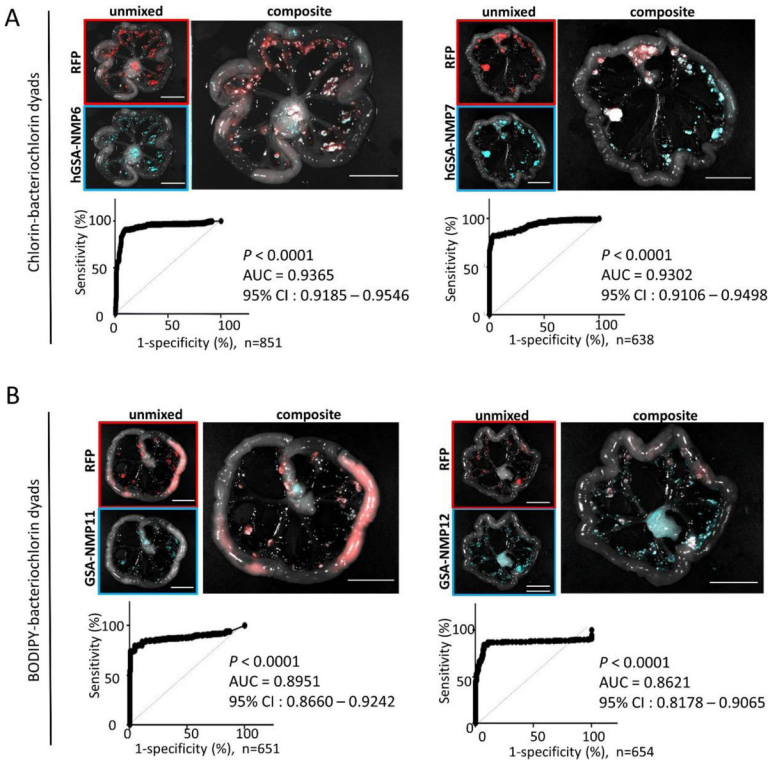


**Figure 3.**

*In vivo* studies of RFP-transfected SHIN3 ovarian cancer bearing mice with hGSA-NMP6 and hGSA-NMP7 (A) and with hGSA-NMP11 and hGSA-NMP12 (B). The activatable probes can produce specific and sensitive fluorescence signals from ovarian cancer cells with minimal background from normal tissue. The red signals show RFP and the cyan signals are show hGSA-conjugated probes. The fluorescence signals of the mesenteric membrane are shown separately in different spectrally resolved fluorescence images. Sensitivity and specificity of the probes for detecting around 1 mm ovarian cancers were calculated by examining nodules in each five mice. Bars are 10 mm.

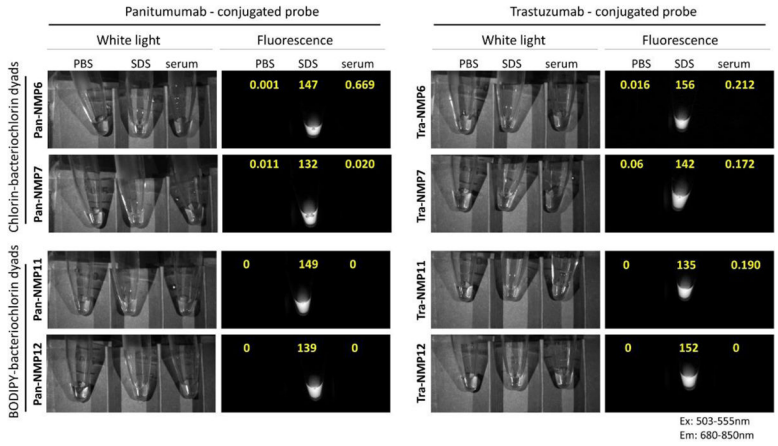


**Figure 4.**

The probes conjugated with a mAb, panitumumab (left) and trastuzumab (right), are self-quenching properties. The former probes specifically bind to EGFR and the latter probes to HER2. Fluorescence quenching properties and stability in serum of all probes are shown. In PBS with 1% SDS, the fluorescence intensities dramatically increase. Numbers (yellow) show mean fluorescence intensity.

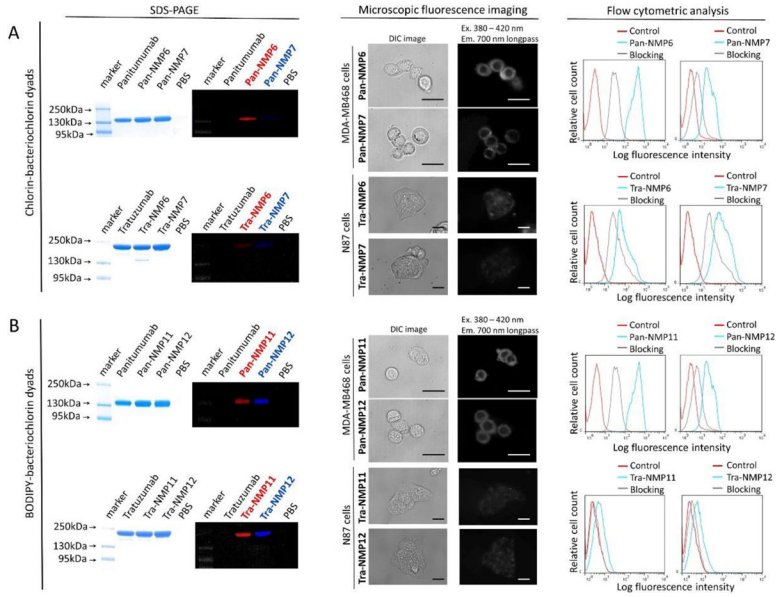


**Figure 5.**

Validation by SDS-PAGE (left: Colloidal Blue staining, right: fluorescence) (left), *in vitro* fluorescence imaging (middle), and flow cytometric analysis (right) of probes conjugated with a mAb, chlorin-bacteriochlorin dyads (A) and BODIPY-bacteriochlorin dyads (B). The signals of fluorescence images in MDA-MB468 cells are detected only in EGFR-expressing cells and those of fluorescence images in N87 cells are in HER2-expressing cells. Bars are 20 μm. To validate the specific binding of the probes to EGFR (upper) or HER2 (lower), excess panitumumab or trastuzumab was used 2 h before overnight incubation of the probes.

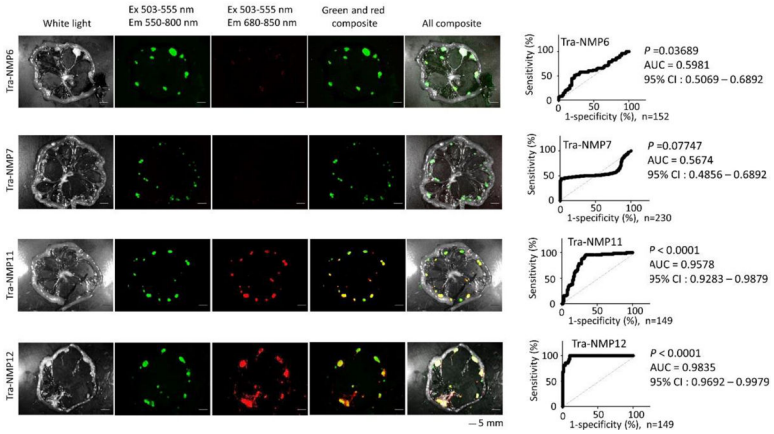


**Figure 6.**

*In vivo* spectral fluorescence imaging of GFP-transfected N87 gastric cancer in the mesentery. The spectral fluorescence image was unmixed, based on the spectral pattern of each probe as well as the GFP pattern and then, composite images consisting of GFP (green), tra-NMP probes (red) were made. Most foci detected by unmixed tra-NMP probe images were co-localized with unmixed GFP positive spots.

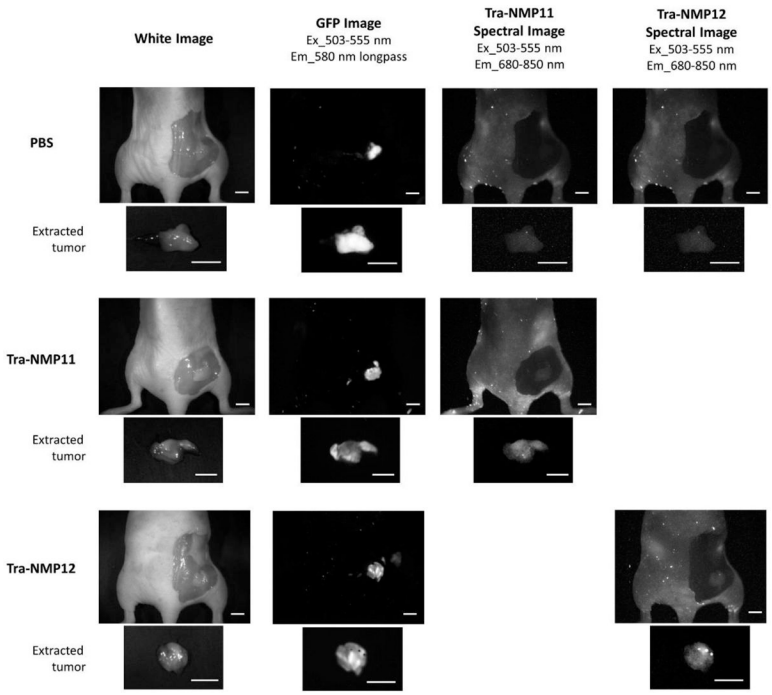


**Figure 7.**

Representative *in vivo* optical images of tra-NMP11 or tra-NMP12 biodistribution after intravenous injection in subcutaneous 3T3Her2_GFP tumor–bearing mice. Upper: control PBS, Middle: tra-NMP11, Lower: tra-NMP12. Excitation is bandpass 503–555 nm, respective emissions are defined with spectral analysis. N = 3 in each group. Bars are 5 mm.

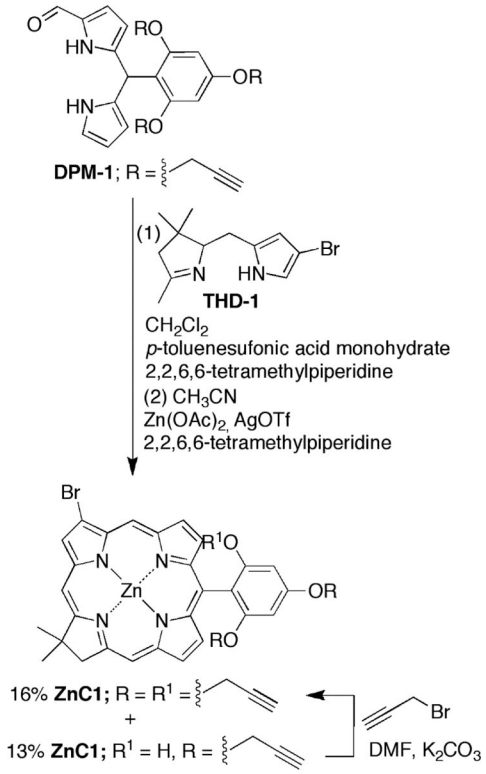


**Scheme 1.**
Synthesis of chlorin containing tris propargyloxy groups

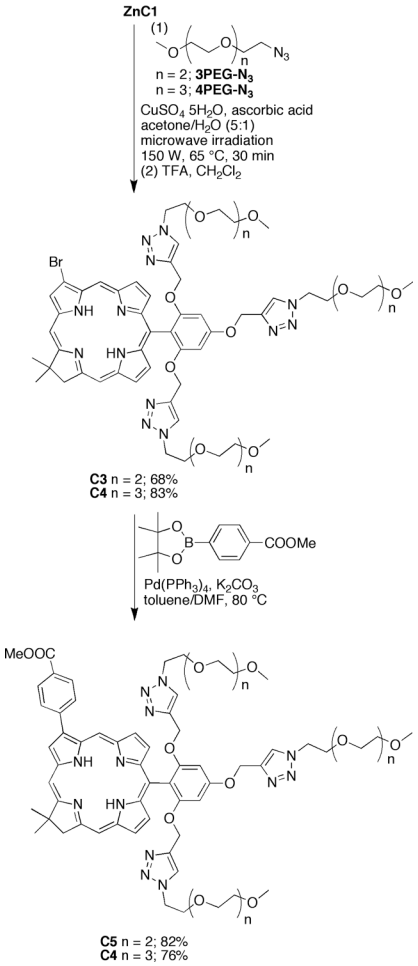


**Scheme 2.**
Synthesis of hydrophilic chlorins

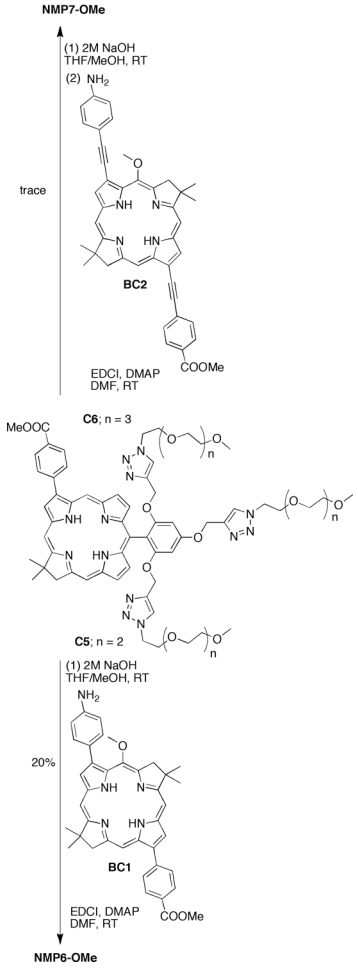


**Scheme 3.**

Synthesis of NMP6-OMe and NMP7-OMe via EDCI-mediated amide formation

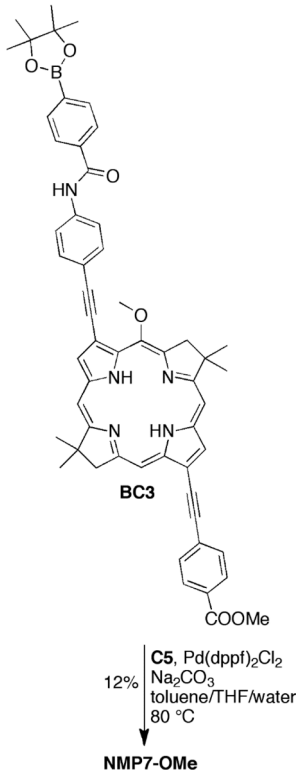


**Scheme 4.**
Synthesis of **NMP7-OMe** via Suzuki reaction

## Table 1

Photophysical characterization on NMP6-OMe and NMP7-OMe

| Dyad | $\lambda_{abs}$ (toluene) | $\lambda_{em}$ (toluene) | $\Phi_f$ (toluene)a ($\lambda_{exc}$) | $\Phi_f$ (DMF)[a] | ETE[b] (toluene) |
|---|---|---|---|---|---|
| **NMP6-OMe** | 372, 417, 513, 647,736 | 744 | 0.20 (513nm) 0.17 (417 ran) | 0.16(515iini) 0.13(418 lira) | 0.85 |
| **NMP7-OMe** | 362, 416, 528, 648, 761 | 767 | 0.26 (531 nm) 0.25 (417 ran | 0.21(530 ran) 0.20(417 ran) | 0.96 |

*a)* Fluorescence quantum yield of bacteriochlorin component,

*b)* energy transfer efficiency, calculated as ETE = $\Phi_{BC}/\Phi_{Ch}$, where $\Phi_{bc}$ and $\Phi_{Ch}$ are fluorescence quantum yields of bacteriochlorin components when bacteriochlorin and chlorin, respectively, arc excitcd.